Supporting Information

Salinity Resistance and Wind-Enhanced Evaporation of Biomass-Derived Foam for Sustainable Solar Desalination

*Wei Wang [a, b *], Xi Huan [a, b, c*], Jingnan Wang [b], Siyuan Kang [a], Yuheng Li [a, d], Ziyu Tian [c *], Yining Li [b], Xue Wang [b], Jiang Fan [b]*

[a] *School of Aeronautical Engineering, Shaanxi Polytechnic University, Xianyang, 712000, China*

[b] *Xianyang Key Laboratory of Solar Thermal Conversion Materials, Shaanxi Polytechnic University, Xianyang, 712000, China*

[c] *School of Opto-electronical Engineering, Xi'an Technological University, Xi'an 710032, China*

[d] *College of Mechanical & Electrical Engineering, Shaanxi University of Science & Technology, Xi'an 710021, China*

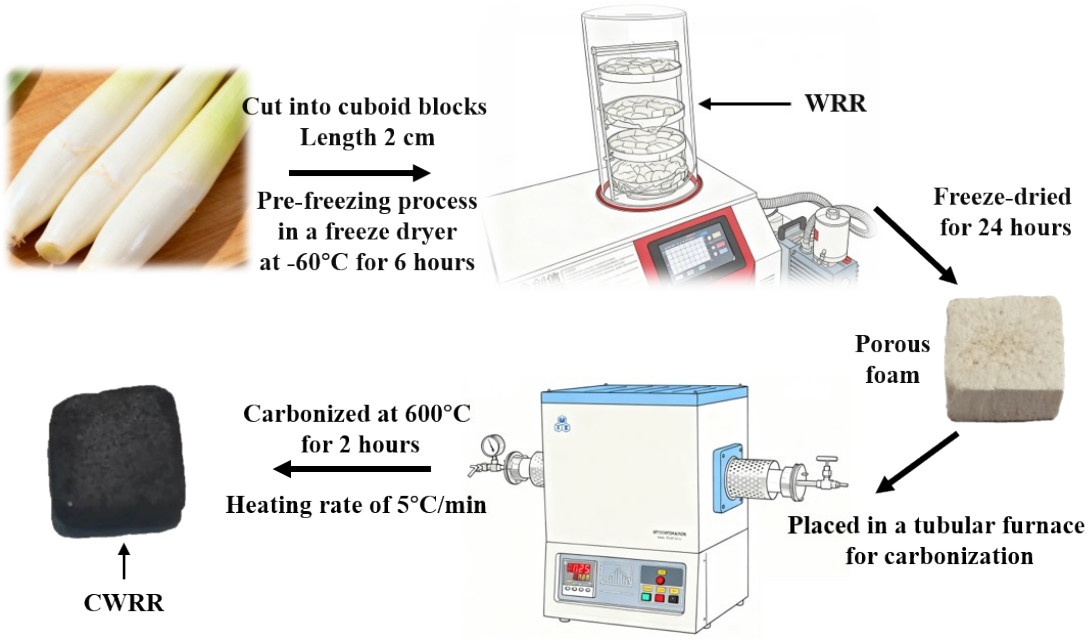

Fig. S1 The preparation process of CWRR

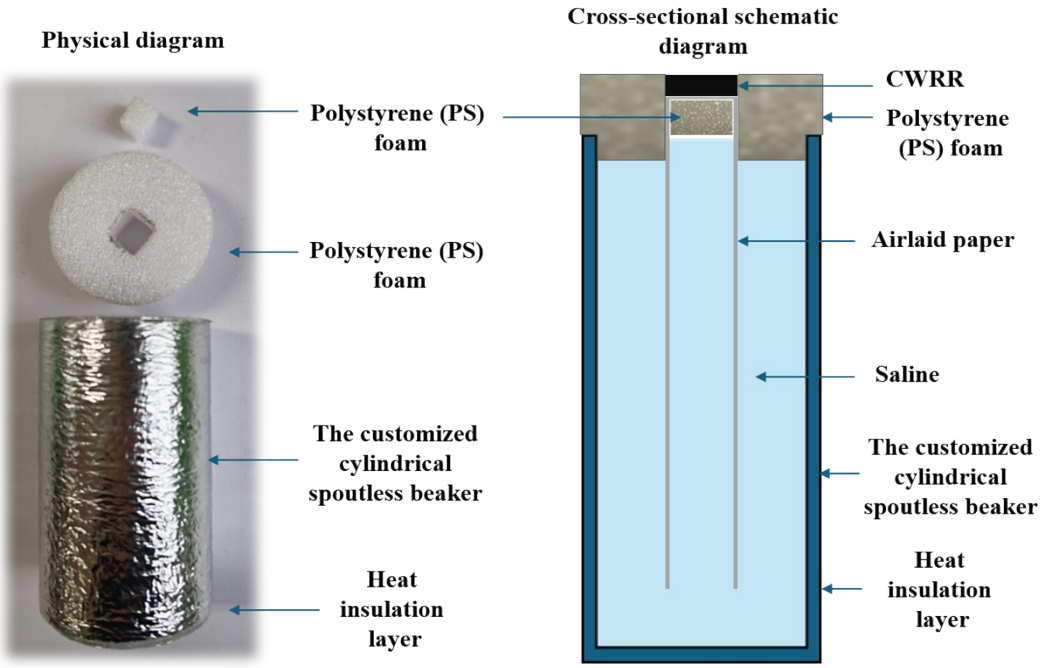

Fig. S2 Physical and cross-sectional schematic diagram of the evaporation device

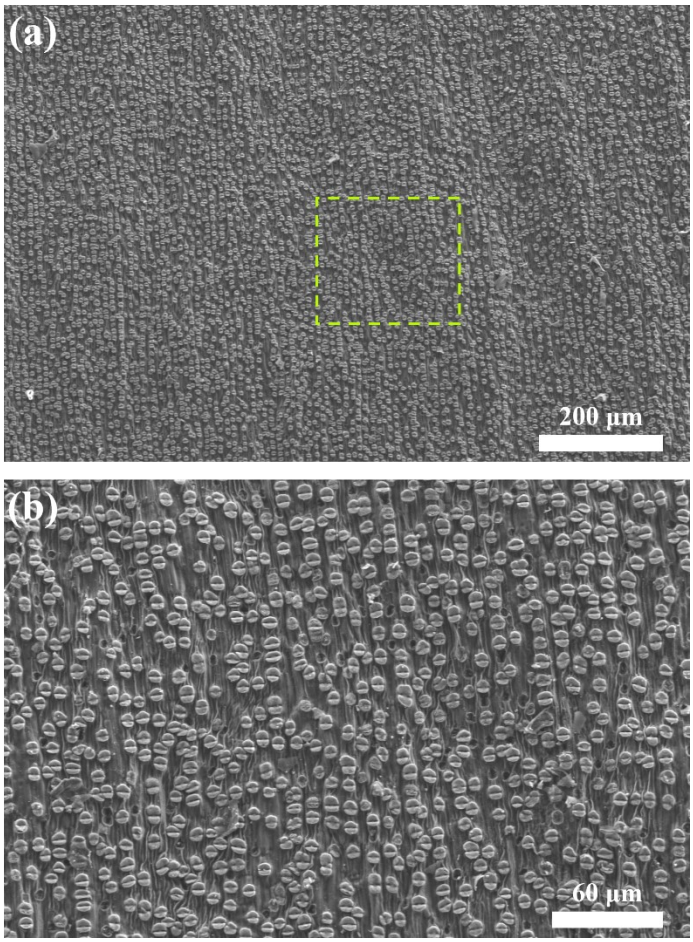

Fig. S3 SEM images of CWRR's (a) side surface and (b) magnified view

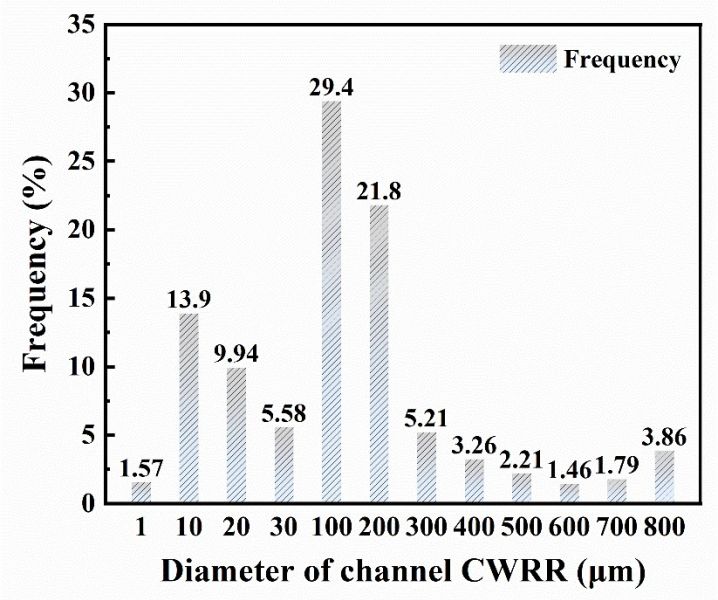

Fig. S4 Diameter distributions of CWRR microchannels

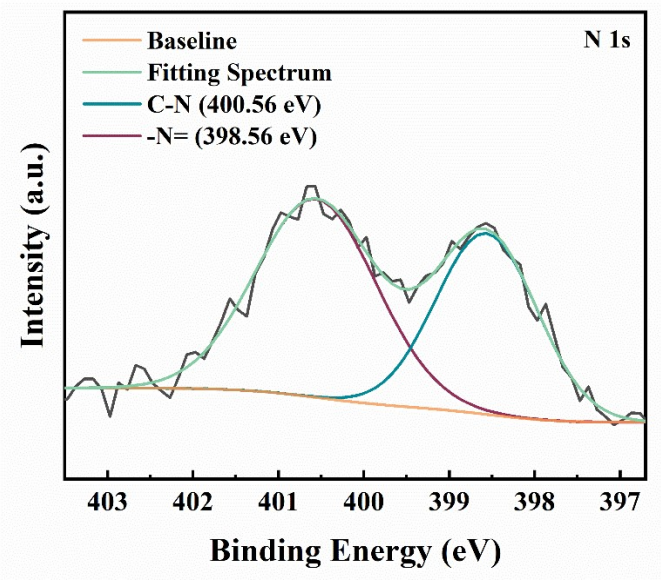

Fig. S5 XPS peak fitting analysis of the N 1s region

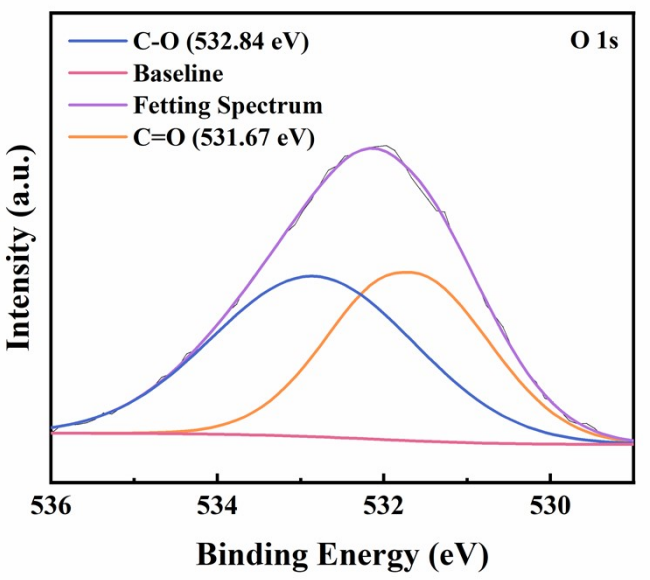

Fig. S6 XPS peak fitting analysis of the O 1s region

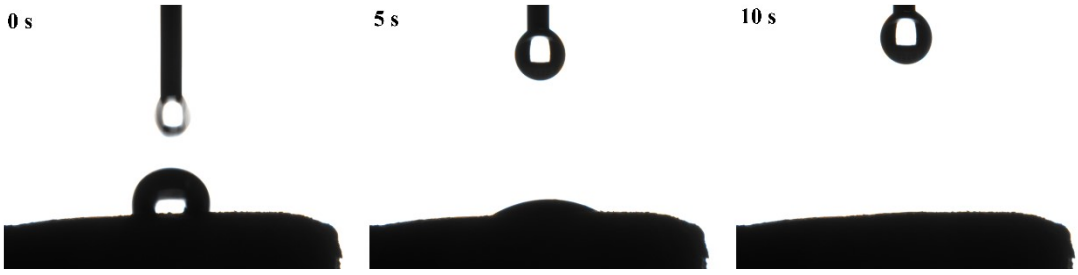

Fig. S7 Water contact angle tests of CWRR

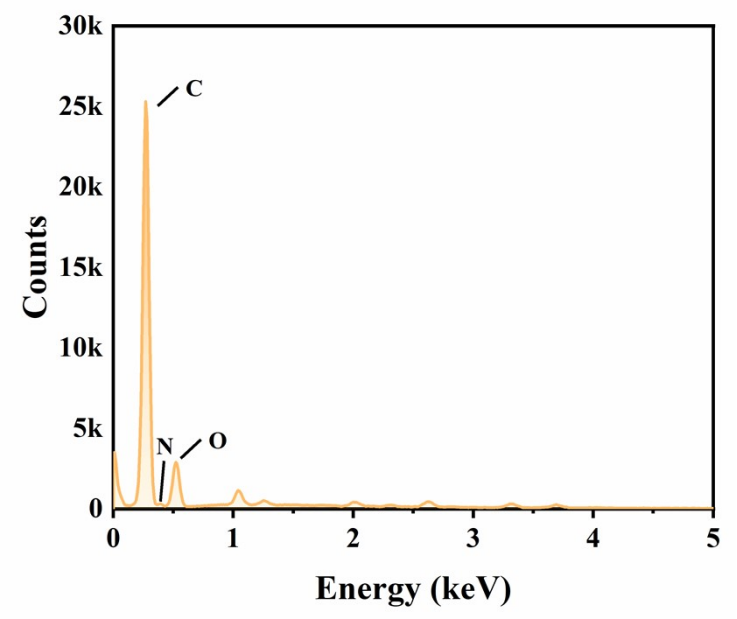

Fig. S8 EDS energy spectrum of CWRR

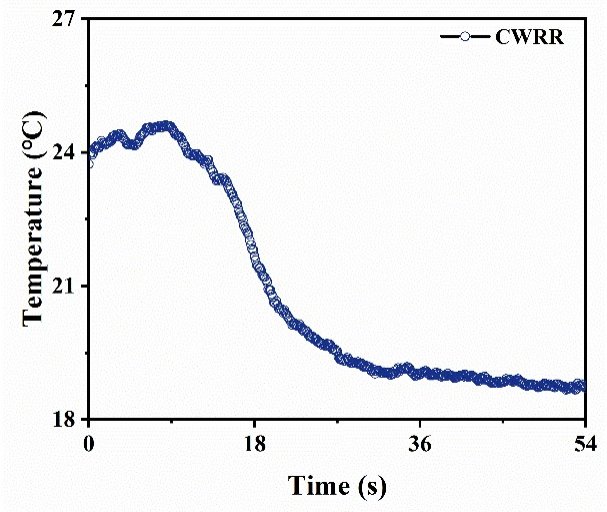

Fig. S9 Surface temperature change during wetting of CWRR in bulk water

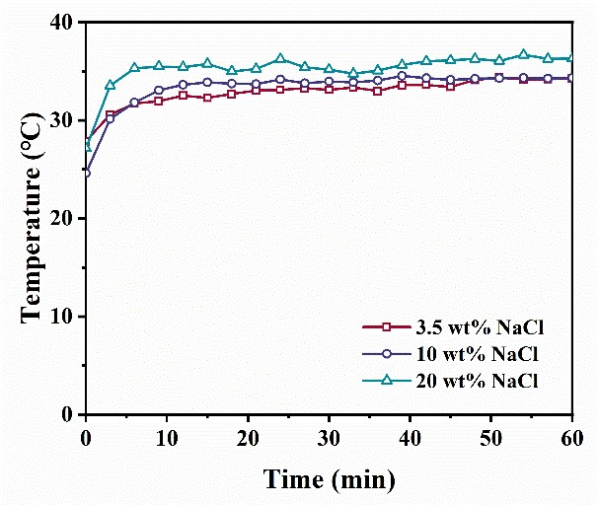

Fig. S10 Surface temperature variations of CWRR during 1-hour evaporation in 3.5-20 wt% NaCl

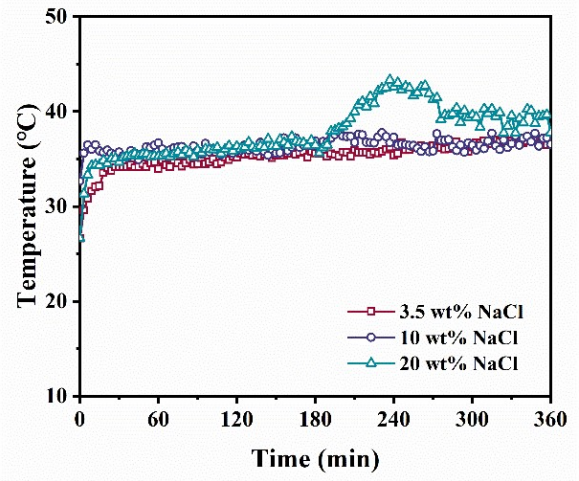

Fig. S11 Surface temperature variations of CWRR during 6-hour evaporation in 3.5-20 wt% NaCl

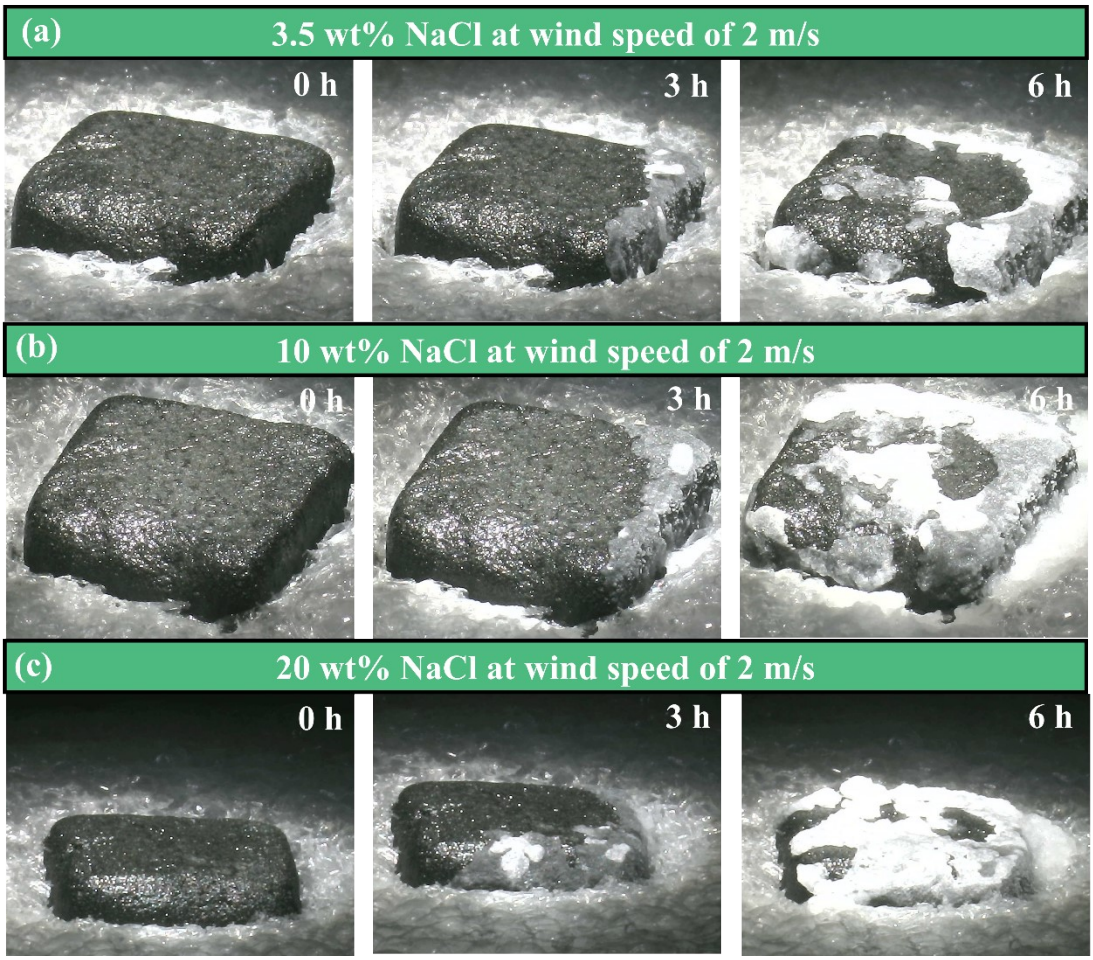

Fig. S12 Digital images of CWRR in (a) 3.5, (b) 10, and (c) 20 wt% NaCl at wind speed of 2 m/s

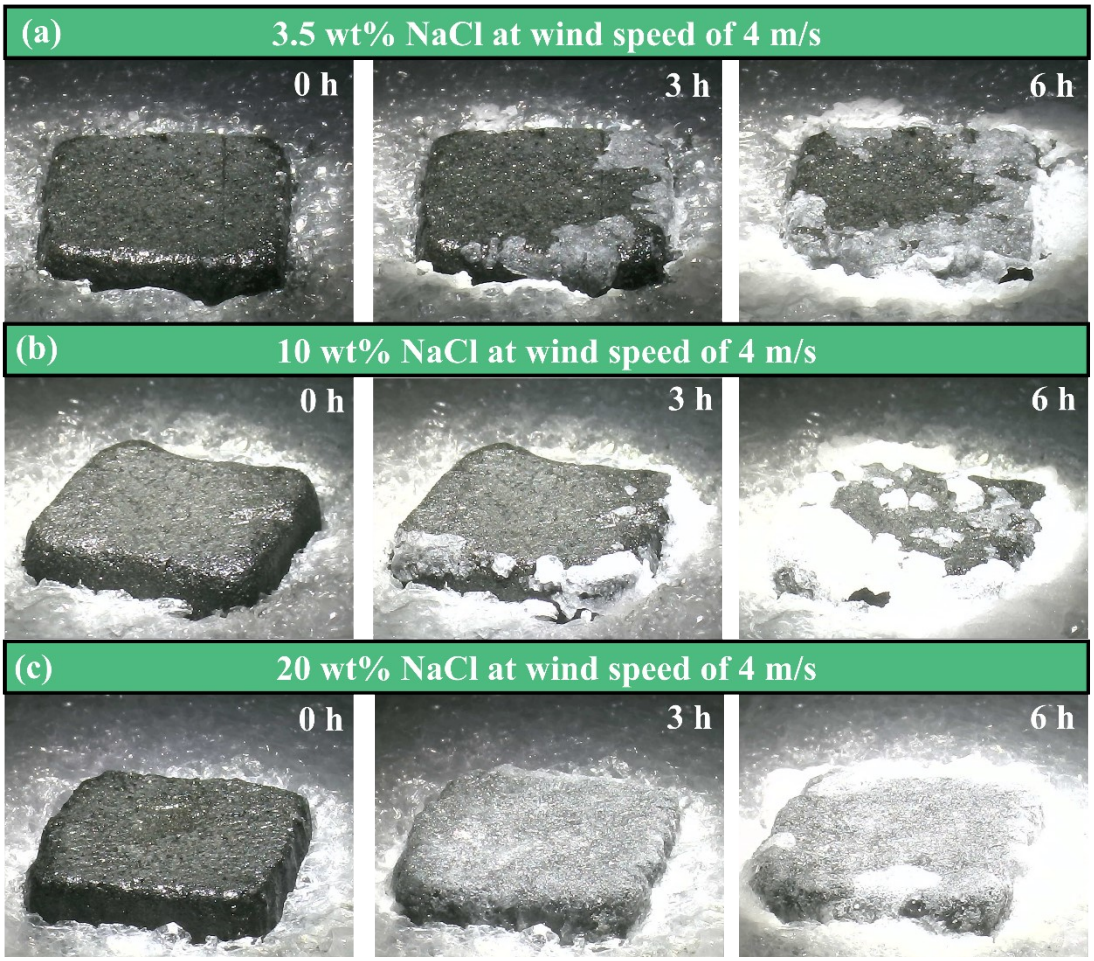

Fig. S13 Digital images of CWRR in (a) 3.5, (b) 10, and (c) 20 wt% NaCl at wind speed of 4 m/s

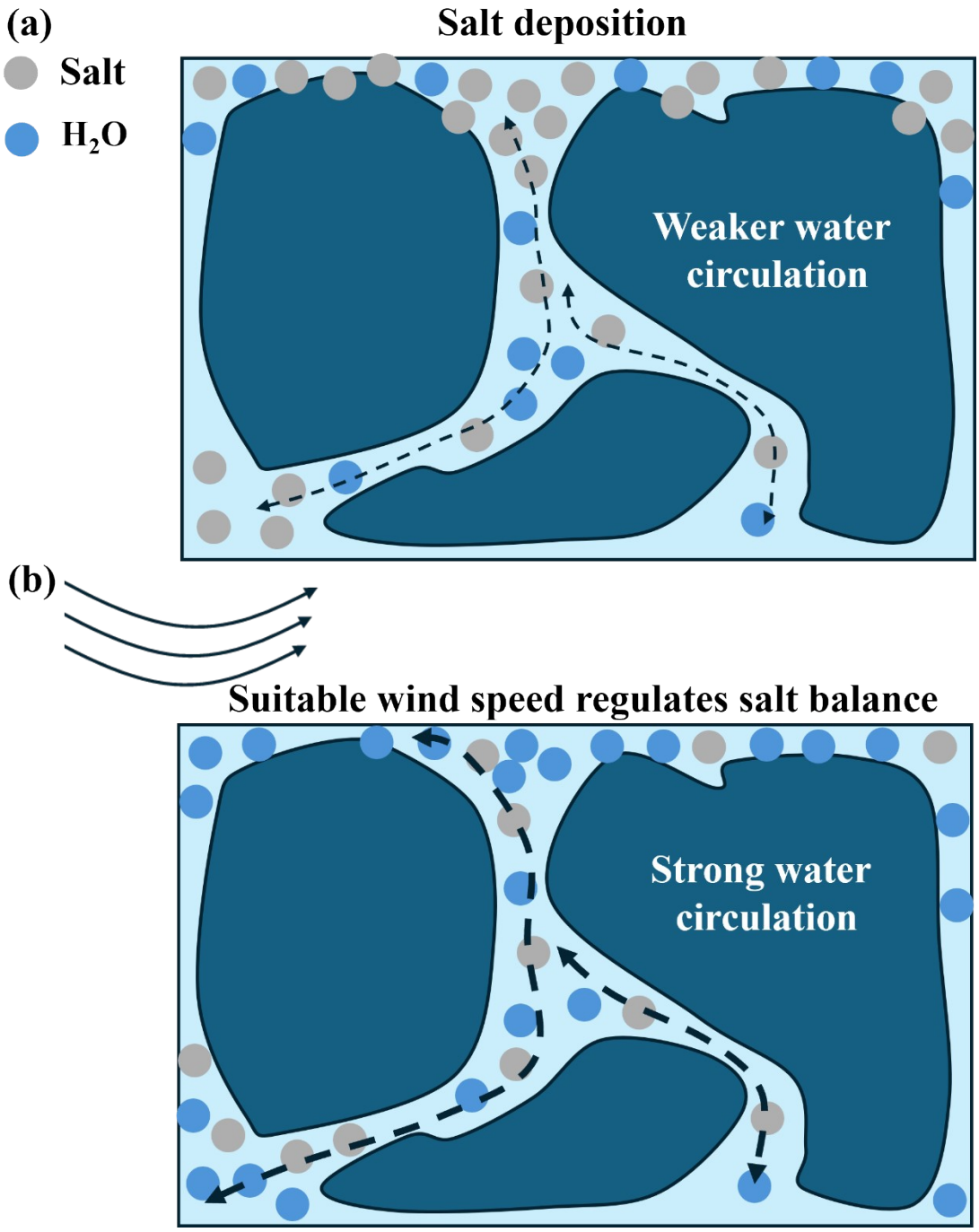

Fig. S14 Schematic diagram of wind speed affecting salt flow inside the evaporator

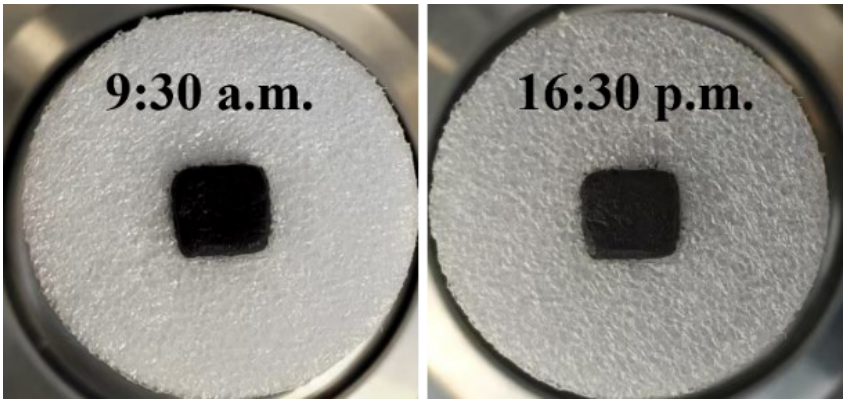

Fig. S15 Digital photographs of CWRR in simulated seawater under natural environment at the initial and final stages of evaporation

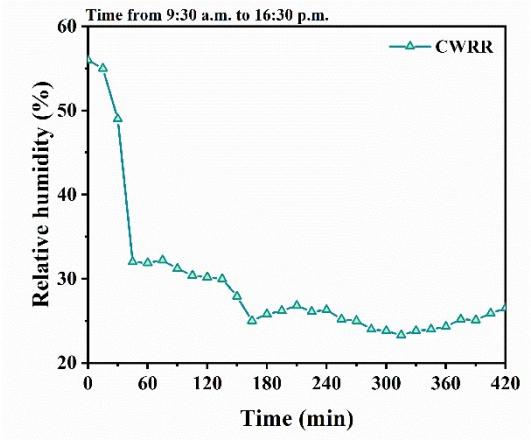

Fig. S16 Relative humidity curve in natural environment from 9:30 a.m. to 16:30 p.m

The calculation formulas for the evaporation rate and efficiency of CWRR.

Evaporation rate and efficiency**:**

$$v = \frac{\Delta m}{A_{proj} \cdot t} \tag{1}$$

where v is the water evaporation rate (kg·m^{-2}·h^{-1}). Δm is the water mass change (kg). A_{proj} is the projected area of the evaporator (m^2). t is the time for solar evaporation (h).

Efficiency and heat loss [1-3]**:**

$$\eta = \frac{Q_{solar} - Q_{rad} - Q_{conv} - Q_{cond}}{c_{opt} \times J_{in} \times A_{proj}} \tag{2}$$

$$Q_{solar} = c_{opt} \times J_{in} \times \alpha \times A_{proj} \tag{3}$$

$$Q_{rad} = A_1 \varepsilon \sigma \left(T_1^4 - T_E^4\right) \tag{4}$$

$$Q_{conv} = A_1 h \left(T_1 - T_E\right) \tag{5}$$

$$Q_{cond} = Cm\Delta T_{water} \tag{6}$$

where η is the solar–thermal conversion efficiency. Q_{solar} is the energy absorbed by the evaporator. c_{opt} is optical concentration. J_{in} is a standard sunlight intensity (1 kW·m^{-2}). A_{proj} is the projected area of the evaporator. Q_{rad} is the radiation heat loss of the evaporator. A_1 are the top evaporation areas. ε is the emissivity of the evaporator in the wavelength of 2.5-25 μm. σ is the Stefan-Boltzmann constant (5.67×10^{-8} W·m^{-2}·K^{-4}). T_1 are the top surface temperatures of the evaporator. T_E is the ambient temperature. Q_{conv} is the convection heat loss. h is the convective heat transfer coefficient, h=5 W·m^{-2}·K^{-1}. Q_{cond} is conduction heat loss. C is the specific heat capacity of water (4.18 J·g^{-1}·K^{-1}). m is the mass of evaporated water within the device. ΔT_{water} is the difference in temperature change of bulk water before and after evaporation.

To avoid the transfer of heat energy from the evaporator to the bulk water, polystyrene (PS) foam was used as a thermal insulation layer to avoid conduction heat loss (**Fig. S2**). Therefore, the temperature difference of the bulk water can be negligible.

The specific data were provided below so that they can be reproduced by researchers. A_1 and A_{proj} are both 0.0004 m^2. The average surface temperatures of CWRR in 3.5, 10, and 20 wt% NaCl during 1 h evaporation were 306.15, 306.42, and 308.33 K, respectively. The average surface temperatures of CWRR in 3.5, 10, and 20 wt% NaCl during 6 h evaporation were 309.5, 308.46, and 310.92 K, respectively.

Under 20 wt% NaCl and 1 m/s airflow, the CWRR's average surface temperatures were 299.57 K (3.5 wt% NaCl), 299.94 K (10 wt% NaCl), and 301.85 K (20 wt% NaCl). At 2 m/s airflow, the average surface temperatures were 297.96 K (3.5 wt%), 297.79 K (10 wt% NaCl), and 300.29 K (20 wt% NaCl). At 4 m/s airflow, the average surface temperatures were 299.15 K (3.5 wt% NaCl), 301.39 K (10 wt% NaCl), and 303.92 K (20 wt% NaCl). The above data can be inserted into Eqs. (2)-(6) to calculate the energy utilization efficiency of the CWRR.

References

[1] J. H. Zhou, Y. F. Gu, P. F. Liu, P. F. Wang, L. Miao, J. Liu, A. Y. Wei, X. J. Mu, J. L. Li, J. Zhu, Development and evolution of the system structure for highly efficient solar steam generation from zero to three dimensions, *Adv. Funct. Mater.* **2019**, 29, 1903255.

[2] N. Xu, X. Z. Hu, W. C. Xu, X. Q. Li, L. Zhou, S. N. Zhu, J. Zhu, Mushrooms as efficient solar steam-generation devices, *Adv. Mater.* **2017**, 29, 1606762.

[3] X. Wu, Z. Q. Wu, Y. D. Wang, T. Gao, Q. Li, H. L. Xu, All-cold evaporation under one sun with zero energy loss by using a heatsink inspired solar evaporator, *Adv. Sci.* **2021**, 8, 2002501.